International Journal of Mechanical Sciences 218 (2022) 107065

Contents lists available at ScienceDirect

International Journal of Mechanical Sciences

journal homepage: www.elsevier.com/locate/ijmecsci

Vacancy dependent mechanical behaviors of high-entropy alloy

Jing Peng [a], Baobin Xie [a], Xin Zeng [a], Qihong Fang [a,*], Bin Liu [b], Peter K. Liaw [c], Jia Li [a,*]

[a] State Key Laboratory of Advanced Design and Manufacturing for Vehicle Body, College of Mechanical and Vehicle Engineering, Hunan University, Changsha, 410082, China
[b] State Key Laboratory of Powder Metallurgy, Central South University, Changsha, 410083, China
[c] Department of Materials Science and Engineering, The University of Tennessee, Knoxville, TN 37996, United States of America

ARTICLE INFO

Keywords:
High entropy alloy
Vacancy
Mechanical properties
Deformation mechanism
Molecular dynamic
Machine learning

ABSTRACT

An abundance of defects would be inevitably generated during manufacturing and service in high-entropy alloys (HEAs). However, the mechanical properties of the damaged HEAs with nanoscale defects have been rarely considered. Meanwhile, an additional challenge is a dearth of the effective reliable method for an in-depth study of damaged HEAs, due to the restriction of the complicated experimental measurement. Here, the effect of zero-dimensional defect, such as vacancy, on mechanical properties in FeNiCoCrCu HEA is studied through the method combining molecular dynamics simulation with machine learning. Atomic simulation results show that the existence of vacancy clusters breaks the continuity of stacking faults and dislocations, and the high vacancy concentrations reduce the strength due to the increase of stacking fault spacing at room temperature. Compared with traditional alloys, HEAs can reduce the property reduction when vacancy exits there. In addition, the anisotropy of vacancy effect is found. The effect of vacancy on the yield strength is more obvious under [100] loading direction than that under the [110] and [111] loading direction. The discrepancy of the stair-rod partial dislocation proportion would be regarded as the primary reason for different yield strengths. The change of vacancy concentration has a significant effect on the deformation mechanism in [100] direction, which is different from that in the [110] and [111] direction. Meanwhile, the effects of vacancy concentration in combination with temperature on the yield strength and dislocation density at yield point of the FeNiCoCrCu HEA are predicted by machine learning, which is on the basis of a set of data obtained from molecular dynamics simulations. The current work provides valuable guidance for HEA design based on the viewpoint of defect regulation.

1. Introduction

High-entropy alloys (HEAs), which follow a characteristic alloying-design concept compared to traditional alloys, have been widely studied owing to their excellent mechanical properties, such as synergetic strength and ductility, great thermal stability and high corrosion resistance [1–5]. In the process of preparation or service, an enormous number of defects are produced inevitably. For example, the vacancy is always reported in HEAs [6–8], which would affect material properties during the process of proliferation and annihilation [9].

As well know, the formation, concentration, and distribution of vacancy play key roles in the microstructures and mechanical properties [9–14]. Such as the previous study, due to the collision of high-energy particles, vacancies and vacancy clusters are induced, resulting in harmful vacancy expansion in HEA [8]. The vacancies introduced by the cyclic deformation improve the strength and ductility of Al alloys through adjusting the dynamic precipitation of solute cluster [10]. The vacancy clusters and vacancy loops are formed by vacancy clustering in the irradiated W, which cause the radiation hardening [11]. Due to the anisotropy of vacancy diffusion, the prismatic interstitial dislocation loop parallel to the base is easier to form in high-purity Zr alloy [12]. There are higher concentration vacancy defects in the HEA than that in traditional alloy, which is regarded as a typic characteristic of the HEA. Thus, the HEA has a strong ability to absorb He atoms and resist irradiation embrittlement, and the influence of these vacancies are similar to oxide in ODS steel [7]. Meanwhile, the existence of vacancy near the crack changes the fracture behavior of material by passivating the crack tip [13]. In GeSbTe alloy, a huge number of atomic vacancies are generated and orderly distributed during the process of rapid crystallization and thermal annealing. However, the vacancy disordering process is observed due to the electron irradiation, which is accompanied by phase transition [14, 15]. Some simulations on the effect of vacancy

* Corresponding authors.
E-mail addresses: fangqh1327@hnu.edu.cn (Q. Fang), lijia123@hnu.edu.cn (J. Li).

https://doi.org/10.1016/j.ijmecsci.2022.107065
Received 23 September 2021; Received in revised form 28 December 2021; Accepted 1 January 2022
Available online 7 January 2022

concentration on mechanical properties are carried out. By studying the effects of vacancy concentration and temperature in single crystal γ-TiAl, the ultimate stress and elastic modulus decrease nonlinearly with the increase of temperature and vacancy concentration [16], but this study focuses on traditional metal, and the range vacancy concentration and temperature are limited. The time-dependent mechanical behavior is found due to the evolution of vacancy concentration and distribution through simulation of the vacancy clustering processes [17]. However, the effect of vacancy on the mechanical properties of HEAs has not been explored at atomic level, which would be affected their industrial applications.

Recently, machine learning has been considered as not only a branch of artificial intelligence, but also a pivotal computer technology in the era of big data. Now, they have been applied in material science [18–23]. Machine learning is used to predict the mechanical properties of existing materials. The fretting crack length and corresponding stress intensity factor of C-Mn steel are predicted by a neural network model, and crack arrest conditions are summarized [19]. The correlation between the process parameters and mechanical properties of industrial steel is established by a deep learning model, which can guide the production of steel with customized mechanical properties [20]. By collecting the data of hundreds of complex concentrated alloys with different chemical compositions, three machine learning classification models are developed to find the relationship between different microstructures and mechanical properties [21]. More importantly, machine learning has outstanding performance in the synthesis design of new material, property prediction, and in-depth characterization of material microstructure [22–25]. Using different machine learning algorithms, the new design parameters are explored for developing a series of alloys out of the FeCrNiZrCu system [22]. A machine learning design system has been proposed, which contains a property-composition BP neural network (NN) model to design the compositions and a composition-property BP NN model to efficiently screen the alloy composition design schemes [23]. Thus, a high-performance Cu alloys with ultimate tensile strength of 600–950 MPa are designed. By statistically analyzing the solidification characteristics of HEAs, the relationship between solidification interval characteristics and element is revealed via machine learning, and the $FeCrNiAl_{0.8}$ HEA is designed, which exhibits a high fracture strength and ductility [24]. The data mining with machine learning is used to reveal the eutectic formation in HEAs, and the critical element of Al is discovered in AlCoCrFeNi system [26]. Meanwhile, if the data is scarce and the experiment is uneconomical, the MD simulation is used as an auxiliary method to provide data sets for machine learning [27, 28].

During this investigation, the uniaxial tensile of single crystal HEAs with vacancies are applied through the MD method. The effects of vacancy concentration on mechanics properties of HEA are analyzed. The crystal orientation effect for different vacancy concentrations is further revealed. Moreover, the MD simulations combined with machine learning method are used to predict the effect of the vacancy concentration in combination with temperature on yield strength and the corresponding dislocation density.

2. Method

In this section, we introduce in detail how to use the MD simulation method to investigate the mechanical response of uniaxial tension in HEA with vacancies at different temperatures. In addition, the specific details of machine learning model are presented based on the data obtained from MD simulation, in order to explore the relationship between vacancy concentrations and mechanical properties.

2.1. Molecular dynamics

Figure 1(a) shows the elemental distribution in a single-crystal FeNiCoCrCu HEA. Figure 1(b) represents various vacancy concentrations, where the corresponding vacancy concentration is shown in Table 1. The FeNiCoCrCu HEA samples with and without vacancies are built, the sizes of models are $30 \times 30 \times 30$ a^3, where $a = 3.61$ Å is a lattice parameter [29]. In order to create the random equal atomic FeNiCoCrCu HEA structure, Fe (Co, Cr, Cu) atoms are randomly selected, and replace with Ni matrix. To compare with conventional alloys, Inconel 718 Ni-based superalloy is selected as the object, which main elements are Ni, Cr, and Fe with atom fractions of 51, 30 and 19 [30]. The orientations of the x, y, and z axes are [100], [010] and [001], respectively. To introduce vacancies in HEA samples, the atoms can be removed randomly for obtaining a given vacancy concentration, where the vacancy generated includes the single vacancy and double vacancy in our model. In addition, a comparative case for the five samples with different vacancy distributions at a certain vacancy concentration

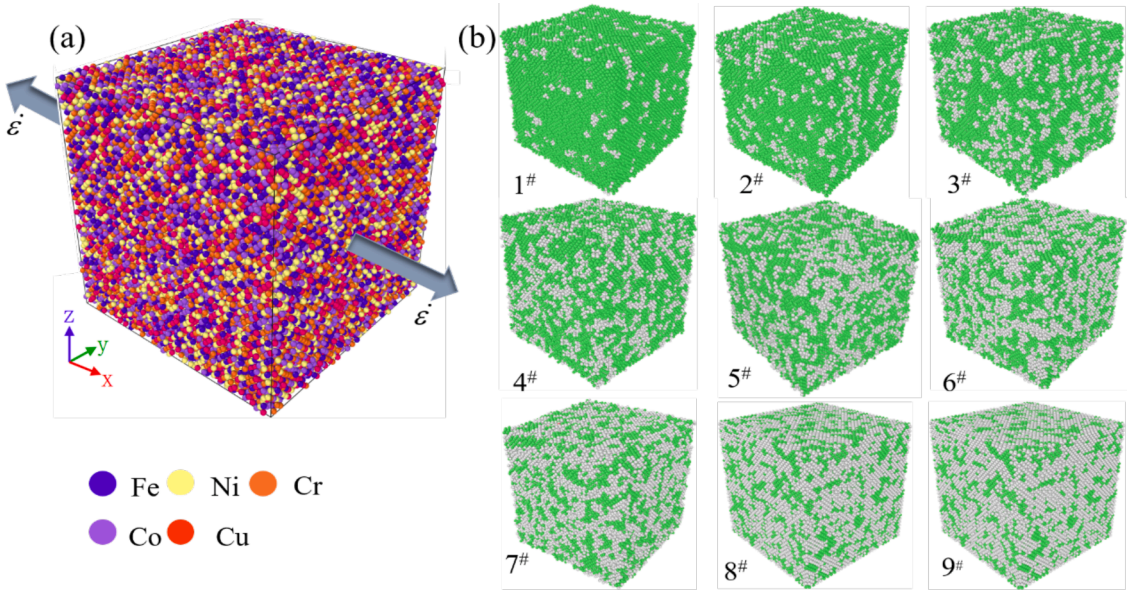

Fig. 1. (a) The uniaxial tensile simulation of FeNiCoCrCu HEA, which atoms are colored by atom type. (b) The vacancy distribution in the FeNiCoCrCu HEA based on CNA method, and the vacancy concentration corresponding to the label is shown in Table 1. Here, Fe Ni Cr Co and Cu in (a), and the green atoms represent FCC structure and the white atoms represent other structure in (b).

Table 1
The vacancy concentration of each graph in Fig. 1(b).

Graphic label	1#	2#	3#	4#	5#	6#	7#	8#	9#
Vacancy concentration (%)	1%	2%	3%	4%	5%	6%	6%	8%	9%

suggests that the random vacancy distribution has a little effect on the mechanical properties. According to previous studies, vacancies as a typical defect of HEAs are distributed in the damaged structure at the initial stage of irradiation due to the collision of high-energy particles [6, 8]. In addition, some studies suggest that the vacancy concentration can reach 10% and disorderly distributed in the material, due to the vacancy formation generated by the processing and deformation of materials [14, 31-33]. For example, when the alloy is irradiated by the electron beam ion, the vacancy distribution changes from order to disorder [14]. Meanwhile, the equipment vacancy concentration can be expressed by $C_v = \exp\left(\frac{\Delta S_f}{R}\right)\exp\left(-\frac{\Delta H_f}{RT}\right)$, where ΔS_f is the formation entropy of the vacancy, R is the Boltzmann constant, ΔH_f is the formation enthalpy, and T is the temperature. The formation enthalpy and formation entropy of HEAs are lower than that in traditional metals, impelling the higher vacancy in HEAs [34, 35]. Thus, the vacancy concentrations fluctuate from 0 to 10%, which be studied with equal intervals of 0.2% for the current simulations.

The deformation of the HEA sample is carried out using LAMMPS [36–39]. All dimensions are applied to periodic boundary conditions. To study the effect of temperature on the deformation behavior, the temperatures of 300 K, 400 K, 500 K, 600 K, 700 K and 800 K are applied in HEA. Firstly, the samples are subjected to the energy minimization using the conjugate gradient method [40–42]; then, they are heated up to the target temperature for a certain time dependent upon the setting temperature under the Nose-Hoover isobaric-isothermal (NPT) ensemble, for obtaining the equilibrium configurations of the vacancy-containing HEAs [38]. After the relaxation, the uniaxial tensile simulation is applied at a strain rate of $1 \times 10^8\ s^{-1}$ along the x direction. The time step of atomic simulation is set to 2 fs. An embedded atom method potential (EAM) is adopted for the atom interactions in FeNiCoCrCu HEA and Ni-based superalloy [42], which is widely used to study their deformation behaviors and mechanical properties [43–46]. Based on the comparison of lattice constant, elastic constant and modulus corresponding to the minimum cohesive energy of FeNiCoCrCu HEA, it is proved that the current EAM potential is sufficient for general research of the mechanical response of stable face-centered cubic (FCC) solid-solution alloy [46]. The database containing temperature, vacancy concentration, yield strength and dislocation density at yield point of the FeNiCoCrCu HEA can be obtained from the tension simulations. The microstructures are analyzed by the common-neighbor analysis (CNA) [47], and their evolutions and defect distributions are presented by the Open Visualization Tool (OVITO) [48]. According to the value of CNA, the green represents FCC atoms, red denotes hexagonal close-packed (HCP) atoms, blue is body-centered cubic (BCC) atoms, and gray represents other disordered atoms.

2.2. Machine learning

In order to predict the relationship between vacancy concentrations and mechanical properties in FeNiCoCrCu HEA, 300 sets of data obtained by MD method are used as the input and output of machine learning. In the machine learning system, the artificial neural network (ANN) is selected. ANN is considered to have sufficient ability to deal with the complex and nonlinear relationship between input data and output data through optimizing hyper-parameter [49], which is hard to be realized by other classical regression algorithms, such as ridge regression, support vector regression and linear regression. Meanwhile, ANN is widely used to explore the relationship between constituent elements, microstructures and mechanical properties of alloy [23, 28]. Figure 2 shows the ANN architecture includes three stages of input, learning, and output. The data input stage includes the data collection and preprocessing. The input dataset is obtained through the tensile simulations of FeNiCoCrCu HEA with various vacancy concentrations under different temperatures. All the vacancy concentration and temperature compose the input data set, and the yield strength and dislocation density constitute the target data set. All the data sets include 300 sets of data, which are divided into training set, test set, and validation set according to the ratio of 70%, 15%, and 15%. Subsequently, the training and learning stages include the process of selecting the appropriate algorithm, adjusting the model structure parameter, training, and testing. The ANN model is built, which contains six components: the number of hidden layers, the number of neurons, the activation function, the optimizer, the training epoch and the learning rate [49, 50]. For the certain amount of data, one hidden layer is adopted due to the accuracy is not improved by increasing the number of hidden layers. Based on the trial-and-error method, the number of neurons is 10 in each layer. Adamoptimizer is employed as the optimizer for model compilation, and 0.01 is used as the learning rate of the adamoptimizer [28]. The unknown data is predicted and analyzed by the optimized model in the final output stage. In our work, the optimized ANN model is used to predict the yield strength and dislocation density in a wide range of vacancy concentration through the dataset obtained by MD simulations.

3. Results and discussion

Based on the method of MD simulation and ANN model, three main contents are discussed in Section 3: (1) the effect of vacancy concentration on tensile properties; (2) the effect of vacancy concentration on the different crystal orientation; (3) the prediction of properties under various vacancy concentrations.

3.1. Effect of vacancy concentration

In this section, the effect of the vacancy concentration in the FeNiCoCrCu HEA on mechanical properties is explored.

The tensile stress-strain curves of MD simulations for the different vacancy concentrations at 300 K have been exhibited in Fig. 3(a, b). The yield strengths extracted from the stress-strain curves are shown in Fig. 3 (c). The previous results show the yield strength of FeNiCoCrCu HEA is about 16 GPa and consistent with 17.2 GPa from our result [51]. The elastic modulus can be computed by the equation of $\sigma = E\varepsilon$, where σ is the axial stress, E is the elastic modulus, and ε is the axial strain. From stress-strain curves in Fig. 3(a, b), the elastic modulus in models decreases slightly with the increase of vacancy concentration, which is similar to the result in traditional alloy [16]. In addition, the yield strength declines tempestuously, and the corresponding strain value also decreases, even for the samples with very low vacancy concentration (Fig. 3(a)) [16]. This phenomenon is most obvious when the vacancy concentration is from 0% to 1%. However, when the vacancy concentration from 1% to 10%, the decline rate of yield strength is relatively uniform.

To deeply understand the effect of vacancy concentration on the deformation behavior in the FeNiCoCrCu HEA sample and quantitatively reveal their mechanical response, the distributions of microstructures are presented in Fig. 4(a–c) [43, 44]. By comparing the microstructure distribution of various samples, a large number of stacking faults (SFs) composed of HCP atoms are generated at the vacancy concentration 0% (Fig. 4(a, b)). The deformation twinning with

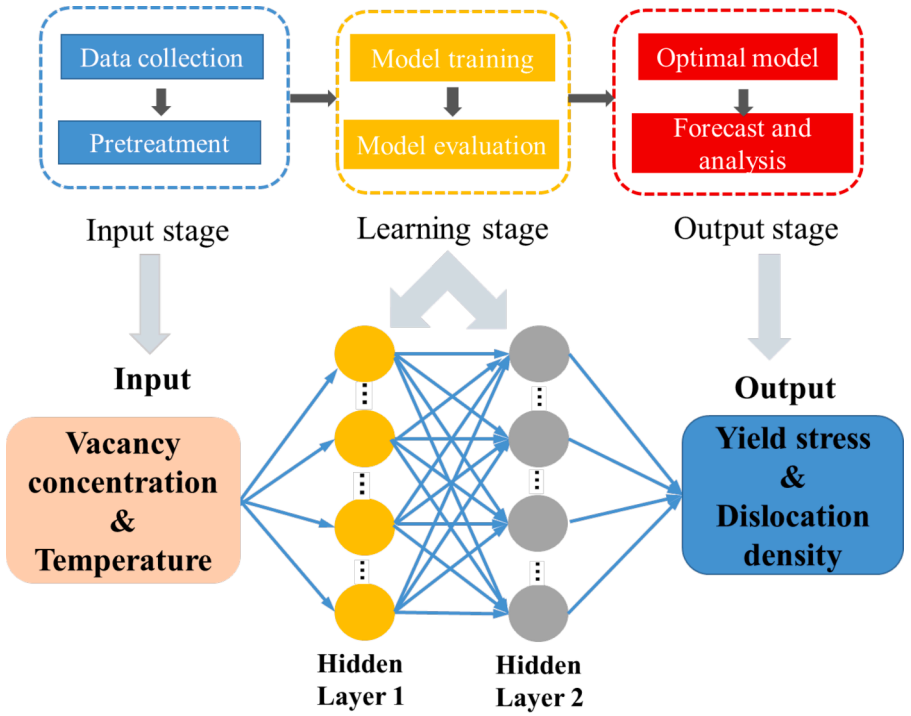

Fig. 2. Workflow chart of machine learning and an architecture of a multi-layer feed-forward ANN.

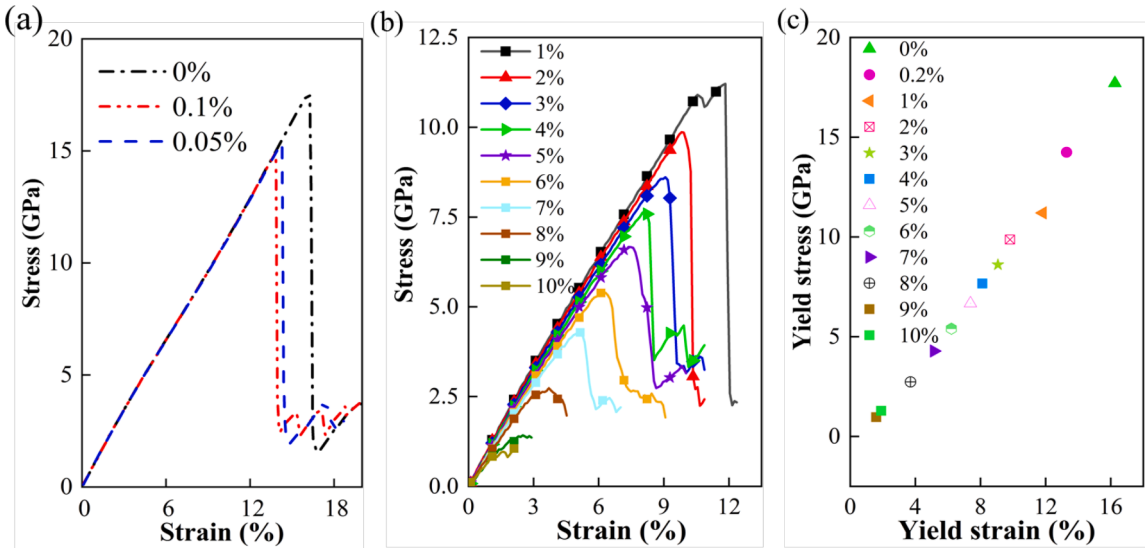

Fig. 3. (a) The tensile stress-strain curve of MD simulations when the vacancy concentrations are lower than 0.1% in the FeNiCoCrCu HEA. (b) The tensile stress-strain curve of MD simulations for vacancy concentrations from 1% to 10% in the FeNiCoCrCu HEA. (c) The relationship between yield stress and yield strain for different vacancy concentration.

very thin thickness is formed in all samples, which induces a weak strengthening effect [52, 53]. Fig. 4(b) shows that the number of SFs and deformation twin is reduced with the increase of the vacancy concentration. Meanwhile, the continuity and thickness of SFs are hindered due to that the aggregation of vacancies into vacancy clusters induces short and dispersive dislocation. The critical pinning stress of dislocation sliding contributed by SFs depends on the SF thickness [54,55]. For the parallel spaced SFs, the SF strengthening can be expressed as $\sigma_{SF} = k/d$ [56], where k is a material constant, and d is the spacing between SFs. The SF strengthening is inversely proportional to the SF spacing, which is one reason for the yield stress has the maximum at the free vacancy concentration (Fig. 3(c)). Corresponding to the distribution of SFs, the number of active slip system is large and a mass of long Shockley partial dislocations are formed, composing intensive dislocation networks at the free vacancy concentration. However, due to the influence of vacancies on the continuity of the slip plane, the short Shockley partial dislocations are formed and constitute sparse dislocation networks in cases with vacancy (Fig. 4(c)). At the intersection of SF planes, more 1/6<110> stair-rod partial dislocations are formed in the structure without vacancies (Fig. 4(c)), and can not slip due to the Burgers vector located in the {001} plane but the slip system of {111}. Hence, the 1/6<110> stair-rod partial dislocations hinder Shockley dislocation slip and influence the deformation behavior, which explains a phenomenon that the strength of perfect sample is higher than that of the other three

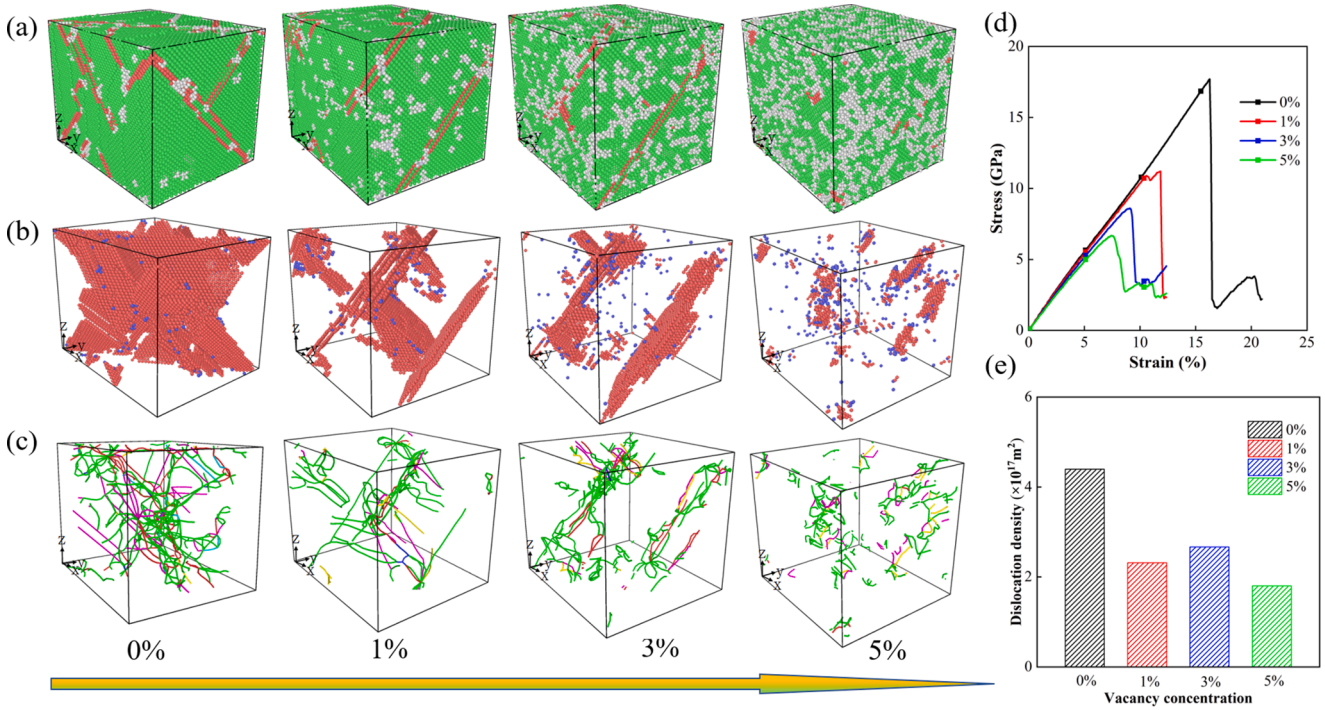

Fig. 4. (a) The microstructure, and (b) defect structure in FeNiCoCrCu HEA at the vacancy concentration of 0%, 1%, 3%, and 5% at yield point. Here, the green atoms represent FCC structure, the red atoms represent HCP structure, the blue atoms represent BCC structure and the white atoms represent other structure. (c) The evolution of dislocation type and distribution, where the green line represents the 1/6<112> Shockley dislocation, the pink line is the 1/6<110> stair-rod dislocation, the blue line denotes the 1/6<110> perfect dislocation, the sky-blue line is the 1/3<111> frank dislocation, and the red line is other dislocation. The stress-strain curve (d), and the dislocation density (e) for various vacancy concentrations. (For interpretation of the references to color in this figure legend, the reader is referred to the web version of this article.)

cases (Fig. 4(d)). Thus, the dislocation mechanism plays an essential role in the hardening mechanism of HEAs [57–59].

Figure 4(e) represents the dislocation densities in the yield point, and the corresponding strains are 17.7%, 11.2%, 8.6%, and 6.7% for the vacancy concentration from 0% to 5%. When the vacancy concentration is high, the vacancy and vacancy clusters are more likely to aggregate during the loading process. This trend causes the dislocation to move violently and the materials enter plastic stage earlier [33]. The

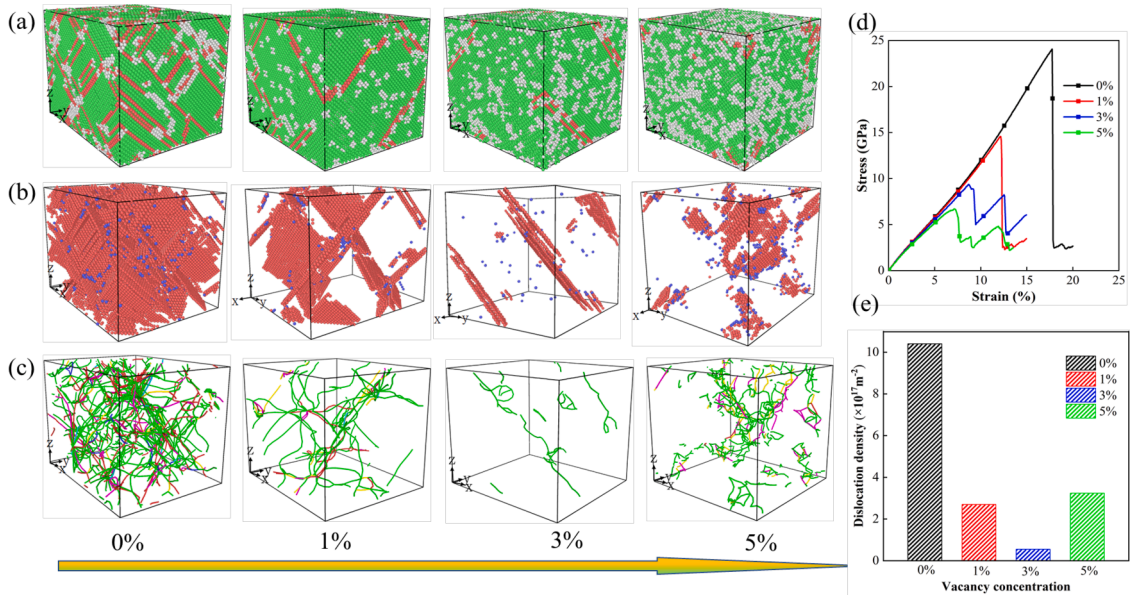

Fig. 5. The microstructure (a), and defect structures (b) in Inconel 718 Ni-based superalloy at the vacancy concentrations of 0%, 1%, 3%, and 5% at yield point. Here, the green atoms represent FCC structure, the red atoms represent HCP structure, the blue atoms represent BCC structure and the white atoms represent other structure. (c) The evolution of dislocation type and distribution, where the green line represents the 1/6<112> Shockley dislocation, the pink line is the 1/6<110> stair-rod dislocation, the blue line denotes the 1/6<110> perfect dislocation, the sky-blue line is the 1/3<111> frank dislocation, and the red line is other dislocation. The stress-strain curve (d), and dislocation density (e) for various vacancy concentrations. (For interpretation of the references to color in this figure legend, the reader is referred to the web version of this article.)

dislocation density of the perfect sample has maximum value at yield point. As the vacancy concentration increase from 0% to 1%, the dislocation density decreases by half. It illustrates the vacancy can inhibit dislocation nucleation and evolution.

In order to study the effect of vacancy on the dislocation density in HEA and conventional alloys, Inconel 718 Ni-based superalloys with 0%, 1%, 3% and 5% vacancy concentration are investigated at 300 K. The microstructures and dislocation distribution at the vacancy concentrations of 0%, 1%, 3%, and 5% are presented in Fig. 5. The change trend of the SFs and deformation twinning is similar in FeNiCrCoCu HEA and Ni-based superalloy with the increase of vacancy concentration. There are higher yield stress and dislocation density in Ni-based superalloy compared that in HEA for vacancy concentration of 0%. However, with the vacancy concentration from 0% to 1%, the dislocation density decreases by about three quarters (Fig. 5(e)), and the yield stress decreases from 24 GPa to 14.58 GPa (Fig. 5(d)), which is more significant than that for FeNiCrCoCu HEA. The phenomenon reveals that compared with traditional alloys, HEAs can weaken the damage effect of vacancy [60].

3.2. Crystal orientation effect

In this section, in order to investigate the effect of vacancy distribution on different crystal orientations, the results of tensile simulations for the FeNiCoCrCu HEA along [100], [110], and [111] directions have been compared.

The stress-strain relations for various crystal orientations at vacancy concentration of 0% and 1% have been shown in Fig. 6. The significantly anisotropy for the three crystal orientations is revealed. For the perfect sample, the yield stress and yield strain are largest on [100] direction. The yield stress for [111] direction is twice that for [110] direction, but the value of yield strain is similar, which is consistent with previous results [51]. In addition, considering the effect of vacancy, the yield stress significantly decreases from 17.9 GPa to 11.2 GPa for the samples with [100] loading direction at the vacancy concentration of 0% to 1%. The elastic modulus decreases slightly [16, 33]. However, the yield stresses are basically not affected by vacancy for the HEA with [110] and [111] loading direction. As a result, the tensile response and the effect of vacancy on tensile property demonstrate the obvious significant anisotropy. The phenomenon is very different from γ-TiAl alloys, whose orientation selection of vacancy is more feeble [60].

The above significant anisotropy is closely related to the microstructure. Figure 7 exhibits the microstructure and dislocation distribution at yield point, revealing the effect of vacancy concentration

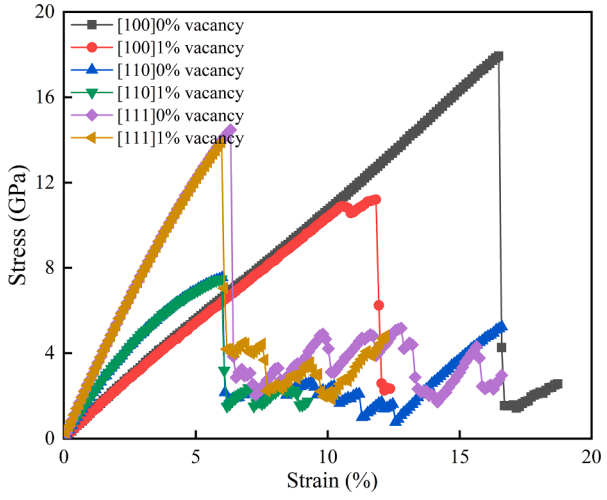

Fig. 6. The stress-strain relations under the [100], [110] and [111] uniaxial loadings at the vacancy concentration of 0% and 1%.

under different crystal orientations. Under the [100], [110], and [111] loadings, the number of the equivalent slip systems to participate in the plastic deformation is 8, 6, and 4 [61]. For the perfect sample under the [100], [110], and [111] loadings, the distribution of slip plane and dislocation as shown in Fig. 7(a, c, e) at yield point. The dislocation slip resistance caused by dislocation interaction is an important part of critical shear stress [57–59]. The more slip systems are actuated, the more likely the slip planes to intersect, so that the more immovable dislocations are generated. Thus, the density of the immovable dislocations (1/6<110> stair-rod partial dislocation) is the highest in Fig. 7 (a) and the smallest in Fig. 7(c). This phenomenon explains that the smallest yield stress under [110] loading direction and the largest yield stress under [100] loading direction in the samples without vacancy (Fig. 6). Meanwhile, when the vacancy concentration increases from 0% to 1%, the number of active slip system and the density of dislocation decrease significantly for [100] direction in Fig. 7(a, b), which corresponds to the significantly decreased yield stress. Comparatively, the change of number and distribution of the slip system and dislocation caused by vacancies is weak for [110] direction (Fig. 7(c, d)) and [111] direction (Fig. 7(e, f)), resulting in basically unchanged yield stress. In addition, the deformation mechanisms are strongly influenced by the crystal orientation and vacancy. Under [100] loading direction, the deformation mechanisms change from dislocation to dislocation coordinated with deformation twinning for the vacancy concentration from 0% to 1%. The dislocation, SF and deformation twinning are the main deformation mechanisms for the [110] loading direction. The dislocation and SF are the deformation mechanisms for [111] loading direction. The change of vacancy concentration has no significant effect on the deformation mechanism for [110] and [111] direction.

3.3. Predicting properties for various vacancy concentrations

In order to guide the optimal design of HEA containing the defects, the properties in defected HEAs should be predicted. Thus, based on a set of data obtained from MD simulation, ANN model is built to predict the evolution of the yield strength and dislocation density under different vacancy concentration and temperature. The combination of two methods can achieve efficient alloy design and performance prediction [27, 28].

Here, the 300 sets of data consisted by the vacancy concentration, yield stress and dislocation density at six different temperatures are obtained through the MD simulations, in which the vacancy concentration in combination with temperature are used as inputs and the yield stress and dislocation density are used as outputs. All the data are divided into the training set, validation set, and test set. Through the ANN model, the correlation between the target data and the prediction data is greater than 0.9 for various data sets, which demonstrates the ANN model used in the current work is extremely accurate.

Figure 8 shows the 3D distribution of the yield stress and dislocation density at different vacancy concentrations and temperatures at yield point obtained from ANN. The distributions are projected to the top of the graphs. When the vacancy concentration is less than 5%, the dislocation density first decreases and then increases slightly (Fig. 8(a)). When the vacancy concentration is greater than 5%, the dislocation density increases sharply at 800 K and reaches a peak. With the vacancy increases, the same phenomenon appears in other temperatures. However, the lower the temperature, the larger the vacancy concentration when the dislocation density increases. The relationship between the yield stress and the vacancy concentration at different temperature obtained from ANN are exhibited in Fig. 8(b). It can be found that with the increase of temperature, the yield stress decreases when the vacancy concentration is less than 6% [38]. After the vacancy concentration is greater than 6%, the yield stress increases and then decreases, which shows a peak. When the temperature is 800 K, the vacancy concentration corresponding to the increase of yield strength is the smallest compared with other temperatures, which is consistent with the

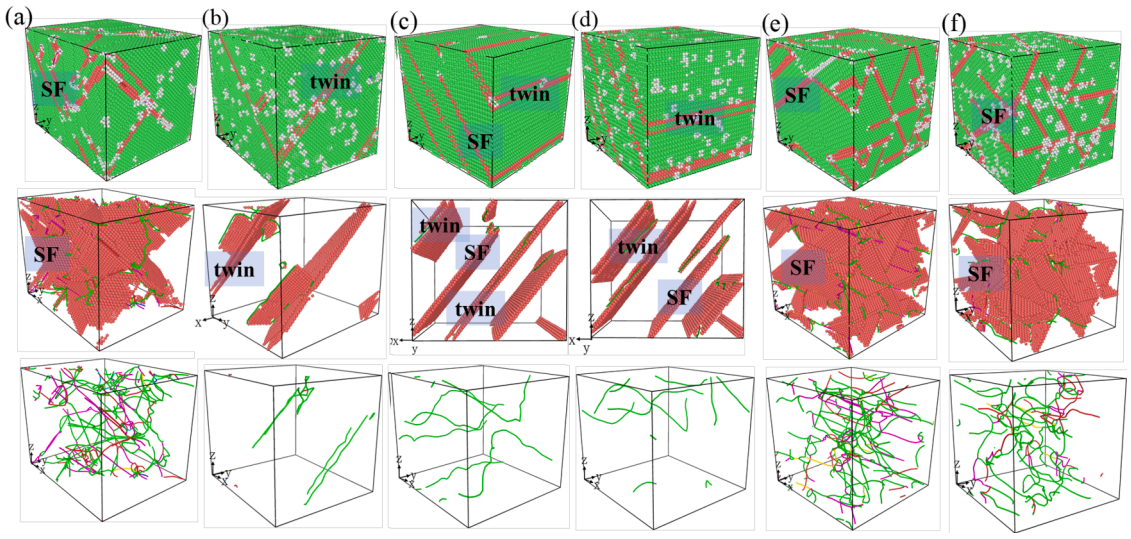

Fig. 7. Snapshots represent the evolution of the microstructure, defect structure and dislocation at yield point of the samples. The crystal orientations are [100]x and [001]z for the perfect sample (a), and the sample with vacancy concentration of 1% (b). The crystal orientations are [110]x and [001]z for the free vacancy (c), and the vacancy concentration of 1% (d). The crystal orientations are [111]x and [11–2]z for the free vacancy (e), and the vacancy concentration of 1% (f).

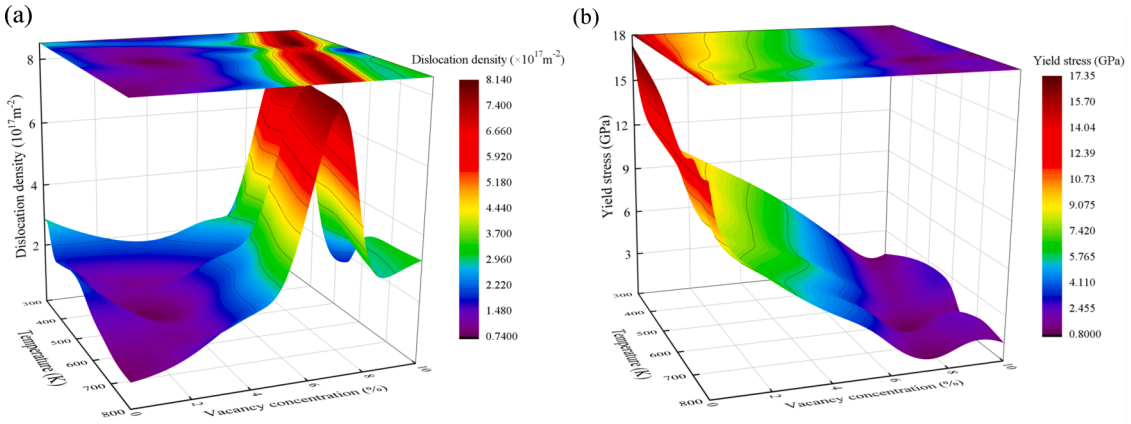

Fig. 8. (a) The distribution of the dislocation density gained from ANN predictions, and (b) the distribution of the yield strengths obtained from ANN predictions under different vacancy concentrations and temperatures.

evolution law of dislocation density in Fig. 8(a).

In order to further compare with the test results of ANN model, some additional validating data is shown in Table 2, which is supplemented by MD simulations and out of the preset dataset. It can be found that the new data is in accord with the predict function, the accuracy of the model has been further verified. Motivated by above reasons and further verifications, the ANN model used in the present work can effectively and accurately obtain the vacancy-property relationship in a wide range of temperature, to provide guidance for the new defected materials.

Table 2
Validating data outside the original data set.

Sample		300 K, 0% [51]	400 K, 41%	500 K, 53%	600 K, 27%	700 K, 13%
Validating results	Yield stress (GPa)	15.5	6.9	4.94	6.96	4.39
	Dislocation density ($\times 10^{17} m^{-2}$)		2.56	2.58	1.27	2.6
Predicted results	Yield stress (GPa)	17.2	6.84	5.1	7.15	4.19
	Dislocation density ($\times 10^{17} m^{-2}$)		2.49	2.01	1.12	2.4

4. Conclusion

In the present work, the effects of the vacancy concentration, crystal orientation and temperature on the tensile properties of FeNiCrCoCu HEA have been systematically investigated by the MD simulation. From the tensile simulation of FeNiCrCoCu HEA with different vacancy concentration, it can be found that the continuity of SFs and dislocations is broken due to the existence of vacancies, and the high vacancy concentration reduces the strength due to the increase of the SF spacing. The increase of vacancy slightly reduces the strength in HEA compared with traditional alloys. In addition, by investigating the effect of vacancy distribution on different crystal orientations, it is found that the yield stress decreases obviously and the deformation mechanism changes from dislocation to dislocation coordinated with deformation twinning with the increase of vacancy concentration for [100] direction. However, the vacancy concentration has no significant effect on the tension stress and deformation mechanism for [110] and [111] direction.

Meanwhile, ANN model is built based on a set of data obtained from MD simulation, thus, the evolution of the yield strength and dislocation

density under different vacancy concentration and temperature in FeNiCrCoCu HEA are predicted efficiently.

These results provide a deep understanding of vacancy effect on mechanical properties. Based on the viewpoint of defect regulation, the present work provides the guidance for the material design.

Data availability statement

The data that supports the results of this research is included in the document.

CRediT authorship contribution statement

Jing Peng: Formal analysis, Software, Investigation, Data curation, Writing – original draft. **Baobin Xie:** Formal analysis, Software, Investigation, Data curation. **Xin Zeng:** Formal analysis, Software. **Qihong Fang:** Conceptualization, Methodology, Validation, Writing – review & editing, Supervision, Funding acquisition. **Bin Liu:** Conceptualization, Validation, Supervision. **Peter K. Liaw:** Writing – review & editing, Project administration, Supervision, Funding acquisition. **Jia Li:** Conceptualization, Methodology, Validation, Writing – review & editing, Supervision, Funding acquisition.

Declaration of Competing Interest

The authors declare that they have no known competing financial interests or personal relationships that could have appeared to influence the work reported in this paper.

Acknowledgments

The authors would like to deeply appreciate the supports from the Foundation for Innovative Research Groups of the National Natural Science Foundation of China (Grant No. 51621004), the National Natural Science Foundation of China (11772122, 51771232, and 11902113), and Natural Science Foundation of Hunan Province (2019JJ50068 and 2021JJ40032). PKL very much appreciates the support from the National Science Foundation (DMR-1611180 and 1809640) with the program directors, Drs. Judith Yang, Gary Shiflet, and Diana Farkas.

References

[1] Yeh JW, Chen SK, Lin SJ, Gan JY, Chin TS, Shun TT, Tsau CH, SY Chang. Nanostructured high-entropy alloys with multiple principal elements: novel alloy design concepts and outcomes. Adv Eng Mater 2004;6(5):299–303.
[2] Li J, Fang Q, Liaw PK. Microstructures and properties of high-entropy materials: modeling, simulation, and experiments. Adv Eng Mater 2020;23(1):2001044.
[3] George EP, Raabe D, Ritchie RO. High-entropy alloys. Nat Rev Mater 2019;4(8):515–34.
[4] Lei Z, Liu X, Wu Y, Wang H, Jiang S, Wang S, et al. Enhanced strength and ductility in a high-entropy alloy via ordered oxygen complexes. Nature 2018;563(7732):546–50.
[5] Yang YC, Liu C, Lin CY, Xia Z. The effect of local atomic configuration in high-entropy alloys on the dislocation behaviors and mechanical properties. Mater Sci Eng A 2021;815:141253.
[6] Lin Y, Yang T, Lang L, Shan C, Deng H, Hu W, Gao F. Enhanced radiation tolerance of the Ni-Co-Cr-Fe high-entropy alloy as revealed from primary damage. Acta Mater 2020;196:133–43.
[7] Lu Y, Huang H, Gao X, Ren C, Gao J, Zhang H, Zheng S, Jin Q, Zhao Y, Lu C, Wang T, Li T. A promising new class of irradiation tolerant materials: Ti2ZrHfV0. 5Mo0. 2 high-entropy alloy. J Mater Sci Technol 2019;35(3):369–73.
[8] Lu C, Niu L, Chen N, Jin K, Yang T, Xiu P, Zhang Y, Gao F, Bei H, Shi S, He MR, Robertson IM, Weber WJ, Wang L. Enhancing radiation tolerance by controlling defect mobility and migration pathways in multicomponent single-phase alloys. Nat Commun 2016;7(1):1–8.
[9] Xu Q, Guan HQ, Zhong ZH, Huang SS, Zhao JJ. Irradiation resistance mechanism of the CoCrFeMnNi equiatomic high-entropy alloy. Sci Rep 2021;11(1):1–8.
[10] Sun W, Zhu Y, Marceau R, Wang L, Zhang Q, Gao X, et al. Precipitation strengthening of aluminum alloys by room-temperature cyclic plasticity. Science 2019;363(6430):972–5.
[11] Cui MH, Shen TL, Zhu HP, Wang J, Cao XZ, Zhang P, et al. Vacancy like defects and hardening of tungsten under irradiation with He ions at 800 °C. Fusion Eng Des 2017;121:313–8.
[12] Christiaen B, Domain C, Thuinet L, Ambard A, Legris A. Influence of vacancy diffusional anisotropy: understanding the growth of zirconium alloys under irradiation and their microstructure evolution. Acta Mater 2020;195:631–44.
[13] Chandra S, Kumar NN, Samal MK, Chavan VM, Patel RJ. Molecular dynamics simulations of crack growth behavior in Al in the presence of vacancies. Comp Mater Sci 2016;117:518–26.
[14] Jiang TT, Wang XD, Wang JJ, Zhou YX, Zhang DL, Lu L, Jia CL, Wuttig M, Mazzarello R, Zhang W. In situ study of vacancy disordering in crystalline phase-change materials under electron beam irradiation. Acta Mater 2020;187:103–11.
[15] Lotnyk A, Bernütz S, Sun X, Ross U, Ehrhardt M, Rauschenbach B. Real-space imaging of atomic arrangement and vacancy layers ordering in laser crystallised Ge2Sb2Te5 phase change thin films. Acta Mater 2016;105:1–8.
[16] Feng RC, Cao H, Li HY, Rui ZY, Yan CF. Effects of vacancy concentration and temperature on mechanical properties of single-crystal γ-TiAl based on molecular dynamics simulation. High Temp Mat Pr 2018;37(2):113–20.
[17] Adibi S, Wilkerson JW. Evolving structure–property relationships in metals with nonequilibrium concentrations of vacancies. J Appl Phys 2020;127(13):135901.
[18] Machaka R. Machine learning-based prediction of phases in high-entropy alloys. Comp Mater Sci 2021;188:110244.
[19] Gorji MB, Pannemaecker A, Spevack S. Machine learning predicts fretting and fatigue key mechanical properties. Int J Mech Sci 2022;215:106949.
[20] Xie Q, Suvarna M, Li J, Zhu X, Cai J, Wang X. Online prediction of mechanical properties of hot rolled steel plate using machine learning. Mater Design 2021;197:109201.
[21] Xiong J, Shi SQ, Zhang TY. Machine learning of phases and mechanical properties in complex concentrated alloys. J Mater Sci Technol 2021;87:133–42.
[22] Zhou Z, Zhou Y, He Q, Ding Z, Li F, Yang Y. Machine learning guided appraisal and exploration of phase design for high entropy alloys. npj Comput Mater 2019;5(1):1–9.
[23] Wang C, Fu H, Jiang L, Xue D, Xie J. A property-oriented design strategy for high performance copper alloys via machine learning. npj Comput Mater 2019;5(1):1–8.
[24] Qiao L, Bao A, Lai Z, Liu Y, Zhu J, Wang Y. Alloy design and properties optimization of multi-component alloy based on solidification characteristics. Mater Sci Eng A 2021;805:140576.
[25] Zhang Y, Wen C, Wang C, Antonov S, Xue D, Bai Y, Su Y. Phase prediction in high entropy alloys with a rational selection of materials descriptors and machine learning models. Acta Mater 2020;185:528–39.
[26] Wu Q, Wang Z, Hu X, Zheng T, Yang Z, He F, Li J, Wang J. Uncovering the eutectics design by machine learning in the Al–Co–Cr–Fe–Ni high entropy system. Acta Mater 2020;182:278–86.
[27] Li L, Xie B, Fang Q, Li J. Machine learning approach to design high entropy alloys with heterogeneous grain structures. Metall Mater Trans A 2021;52(2):439–48.
[28] Li J, Xie B, Fang Q, Liu B, Liu Y, Liaw PK. High-throughput simulation combined machine learning search for optimum elemental composition in medium entropy alloy. J Mater Sci Technol 2020;68:70–5.
[29] An Z, Jia H, Wu Y, Rack PD, Patchen AD, Liu Y, Ren Y, Li N, Liaw PK. Solid-solution CrCoCuFeNi high-entropy alloy thin films synthesized by sputter deposition. Mater Res Lett 2015;3(4):203–9.
[30] Wang HP, Zheng CH, Zou PF, Yang SJ, Hu L, Wei B. Density determination and simulation of Inconel 718 alloy at normal and metastable liquid states. J Mater Sci Technol 2018;34(3):436–9.
[31] Jordan JL, Deevi SC. Vacancy formation and effects in FeAl. Intermetallics 2003;11(6):507–28.
[32] Chang WJ. Molecular-dynamics study of mechanical properties of nanoscale copper with vacancies under static and cyclic loading. Microelectronic Eng 2003;65(1–2):239–46.
[33] Durand A, Peng L, Laplanche G, Morris JR, George EP, Eggeler G. Interdiffusion in Cr–Fe–Co–Ni medium-entropy alloys. Intermetallics 2020;122:106789.
[34] Huang EW, Chou HS, Tu KN, Hung WS, Lam TN, Tsai W, Chiang CY, Lin BH, Yeh AC, Chang SH, Chang YJ, Yang J, Li XY, Ku C, An K, Chang YW, Jao YL. Element effects on high-entropy alloy vacancy and heterogeneous lattice distortion subjected to quasi-equilibrium heating. Sci Rep 2019;9(1):1–10.
[35] Sugita K, Matsuoka N, Mizuno M, Araki H. Vacancy formation enthalpy in CoCrFeMnNi high-entropy alloy. Scripta Mater 2020;176:32–5.
[36] Plimpton S. Fast parallel algorithms for short-range molecular dynamics. J Comp Phys 1995;117:1–19.
[37] Li J, Li L, Jiang C, Fang Q, Liu F, Liu Y, Liaw PK. Probing deformation mechanisms of gradient nanostructured CrCoNi medium entropy alloy. J Mater Sci Technol 2020;57:85–91.
[38] Li L, Chen H, Fang Q, Li J, Liu F, Liu Y, Liaw PK. Effects of temperature and strain rate on plastic deformation mechanisms of nanocrystalline high-entropy alloys. Intermetallics 2020;120:106741.
[39] Bahramyan M, Mousavian RT, Brabazon D. Determination of atomic-scale structure and compressive behavior of solidified AlxCrCoFeCuNi high entropy alloys. Int J Mech Sci 2020;171:105389.
[40] Guénolé J, Nöhring WG, Vaid A, Houllé F, Xie Z, Prakash A, Bitzek E. Assessment and optimization of the fast inertial relaxation engine (fire) for energy minimization in atomistic simulations and its implementation in lammps. Comp Mater Sci 2020;175:109584.
[41] Guan YL, Shao JL, Song WD. Molecular dynamics study on dynamic response of void-included aluminum under different loading patterns. Int J Mech Sci 2020;181:105707.

[42] Farkas D, Caro A. Model interatomic potentials and lattice strain in a high-entropy alloy. J Mater Res 2018;33(19):3218–25.
[43] Luo G, Li L, Fang Q, Li J, Tian Y, Liu Y, Liu B, Peng J, Liaw PK. Microstructural evolution and mechanical properties of FeCoCrNiCu high entropy alloys: a microstructure-based constitutive model and a molecular dynamics simulation study. Appl Math Mech 2021;42(8):1109–22.
[44] Tian Y, Fang Q, Li J. Molecular dynamics simulations for nanoindentation response of nanotwinned FeNiCrCoCu high entropy alloy. Nanotechnology 2020;31(46):465701.
[45] Liu J. Molecular dynamic study of temperature dependence of mechanical properties and plastic inception of CoCrCuFeNi high-entropy alloy. Phy Lett A 2020;384(22):126516.
[46] Tan F, Li J, Feng H, Fang Q, Jiang C, Liu Y, Liaw PK. Entropy-induced transition on grain-boundary migration in multi-principal element alloys. Scripta Mater 2021;194:113668.
[47] Tsuzuki H, Branicio PS, Rino JP. Structural characterization of deformed crystals by analysis of common atomic neighborhood. Comput Phys Commun 2007;177(6):518–23.
[48] Stukowski A. Visualization and analysis of atomistic simulation data with OVITO–the Open Visualization Tool. Model Simul Mater Sci Eng 2009;18(1):015012.
[49] Huang W, Martin P, Zhuang HL. Machine-learning phase prediction of high-entropy alloys. Acta Mater 2019;169:225–36.
[50] Dewangan SK, Samal S, Kumar V. Microstructure exploration and an artificial neural network approach for hardness prediction in AlCrFeMnNiWx High-Entropy Alloys. J Alloy Compd 2020;823:153766.
[51] Held LI. Designing FeNiCr (CoCu) high entropy alloys using molecular dynamics-a study of the enhanced mechanical properties of a novel group of composites. Diss. Rochester Institute of Technology; 2021.
[52] Peng J, Li L, Li F, Liu B, Zherebtsov S, Fang Q, Jia L, Stepanov N, Liu Y, Liu Y, Liaw PK. The predicted rate-dependent deformation behaviour and multistage strain hardening in a model heterostructured body-centered cubic high entropy alloy. Int J Plast 2021;145:103073.
[53] Choudhuri D, Gwalani B, Gorsse S, Komarasamy M, Mantri SA, Srinivasan SG, Mishra RS, Banerjee R. Enhancing strength and strain hardenability via deformation twinning in FCC-based high entropy alloys reinforced with intermetallic compounds. Acta Mater 2019;165:420–30.
[54] Li J, Chen H, Fang Q, Jiang C, Liu Y, Liaw PK. Unraveling the dislocation–precipitate interactions in high-entropy alloys. Int J Plast 2020;133:102819.
[55] Peng Q, Sun Y, Ge B, Fu H, Zu Q, Tang X, Huang J. Interactive contraction nanotwins-stacking faults strengthening mechanism of Mg alloys. Acta Mater 2019;169:36–44.
[56] Jian WW, Cheng GM, Xu WZ, Koch CC, Wang QD, Zhu YT, Mathaudhu SN. Physics and model of strengthening by parallel stacking faults. Appl Phys Lett 2013;103(13):133108.
[57] Li J, Fang Q, Liu B, Liu YW, Liu Y. Mechanical behaviors of AlCrFeCuNi high-entropy alloys under uniaxial tension via molecular dynamics simulation. RSC Adv 2016;6(80):76409–19.
[58] Li Z, Cui Y, Yan W, Zhang D, Fang Y, Chen Y, Yu Q, Wang G, Ouyang H, Fan C, Guo Q, Xiong DB, Jin S, Sha G, Ghoniem N, Zhang Z, Wang YM. Enhanced strengthening and hardening via self-stabilized dislocation network in additively manufactured metals. Mater Today 2021;50:79–88.
[59] Cui Y, Shen J, Manladan SM, Geng K, Hu S. Strengthening mechanism in two-phase FeCoCrNiMnAl high entropy alloy coating. Appl Surf Sci 2020;530:147205.
[60] Li HY, Kou P, Li LL, Feng RC, Cao H. Effect of orientations on tensile property of single crystal γ-TiAl alloys with certain vacancy concentration. Rare Metal Mat Eng 2020;49(5).
[61] Li J, Fang Q, Liu B, Liu Y. Transformation induced softening and plasticity in high entropy alloys. Acta Mater 2018;147:35–41.